INTERNATIONAL JOURNAL OF HYDROGEN ENERGY 45 (2020) 8490–8496

Available online at www.sciencedirect.com

ScienceDirect

journal homepage: www.elsevier.com/locate/he

In-situ formation of Ni (oxy)hydroxide on Ni foam as an efficient electrocatalyst for oxygen evolution reaction

Kai Wan [a], *Jiangshui Luo* [b,c,*], *Xuan Zhang* [a], *Palaniappan Subramanian* [a], *Jan Fransaer* [a,**]

[a] *Department of Materials Engineering, KU Leuven, Leuven, 3001, Belgium*
[b] *College of Materials Science and Engineering, Sichuan University, 610065, Chengdu, China*
[c] *Laboratory for Soft Matter and Biophysics, Department of Physics and Astronomy, KU Leuven, Leuven, 3001, Belgium*

HIGHLIGHTS

- Electrochemical activation method is a time and energy-saving method.
- Strong electronic interaction between NiOOH and Ni favors electron transfer.
- High valence Ni in NiOOH enhances the chemisorption of OH^- during OER.
- In situ formation of NiOOH layer reduces the interfacial electronic resistance.

ARTICLE INFO

Article history:
Received 3 October 2019
Received in revised form
11 December 2019
Accepted 7 January 2020
Available online 1 February 2020

Keywords:
In-situ formation
Electrochemical activation method
Ni (oxy)hydroxide
Oxygen evolution reaction
Durability

ABSTRACT

A binder-free Ni (oxy)hydroxide on Ni foam was prepared through an in-situ electrochemical activation method. Ni (oxy)hydroxide is active for the oxygen evolution reaction. The Ni (oxy)hydroxide directly formed on the surface of Ni foam as a binder-free catalyst not only exhibited large electrochemically active area, but also displayed low interfacial electronic resistance and low charge transfer resistance. Therefore, the optimized Ni (oxy)hydroxide exhibits an overpotential of 288 and 370 mV at 10 and 500 mA cm^{-2}, respectively, in 1.0 M KOH for the oxygen evolution reaction, as well as favorable during 240 h at 100 mA cm^{-2}.

* *Corresponding author*. College of Materials Science and Engineering, Sichuan University, 610065, Chengdu, China
** *Corresponding author*. Department of Materials Engineering, KU Leuven, Leuven, 3001, Belgium
E-mail addresses: kai.wan@kuleuven.be (K. Wan), jiangshui.luo@kuleuven.be (J. Luo), jan.fransaer@kuleuven.be (J. Fransaer).
https://doi.org/10.1016/j.ijhydene.2020.01.043

Introduction

Electrochemical water splitting, which is composed of the hydrogen evolution reaction (HER) and the oxygen evolution reaction (OER), has been regarded as one of the most ideal strategies for the production of hydrogen [1–9]. However, the OER displays a high overpotential (η) because of its sluggish kinetic process even using noble metal-based materials (IrO_2 and RuO_2) as electrocatalysts in alkaline media [10–12]. Therefore, considerable efforts have been devoted to developing low-cost, highly active and stable electrocatalysts [13–18].

In the past decades, transition metal-based oxides, (oxy)hydroxides and sulfides have achieved excellent electrocatalytic activity for the OER in alkaline media [19–25]. For example, Sun et al. prepared serials of nanostructured materials as highly active electrocatalysts for the OER, such as $Co(OH)_2$, Co-doped CuO, Zn-doped Ni_3S_2, Fe-doped $NiCr_2O_4$ [26–29]. Feng et al. fabricated 3D NiCoP@$NiCoPO_x$ core-shell nanostructure and NiCoP-decorated N, S, P-codoped hierarchical porous carbon nanosheet as efficient OER electrocatalysts [30,31]. In addition, recent research indicated that the surface of the Ni-based electrocatalyst is slightly oxidized to Ni^{3+} under OER conditions, which favors the formation of NiOOH [32–34] Liu et al. synthesized Ni–Co oxide hierarchical nanosheets with active NiOOH on the surface, which was considered as the main active sites for the OER [33]. Wan et al. reported a hierarchical porous Ni_3S_4 electrocatalyst with enriched high-valence Ni sites, which exhibited an excellent OER activity [35]. The density functional theory (DFT) calculations confirmed that the presence of Ni^{3+} enhances the chemisorption of OH^-. Despite all this progress, Ni-based electrocatalysts still suffer problems in practical applications, such as insufficient electrocatalytic activity, poor long-term stability due to detachment from the electrode at high current densities, and low electronic conductivity.

To this end, we develop an electrochemical activation method for the *in-situ* formation of Ni (oxy)hydroxide on Ni foam (NF) in a strong alkaline electrolyte (6.0 M KOH). When comparing with other synthesis methods, such as solvothermal/hydrothermal methods, and high-temperature pyrolysis methods, the in-situ electrochemical activation of NF exhibits several advantages. First, the electrochemical activation method is a time and energy-saving method, which is performed at room temperature. Second, the Ni (oxy)hydroxide directly formed on the surface of NF as a binder-free catalyst, which reduced the interfacial electronic resistance [36,37]. Third, the high porosity of NF not only increases the number of active sites on its surface but also favors faster mass transfer [38,39]. As a result, the optimized electrode NF-2 exhibits low overpotentials (η) of 288, 333, 358 and 370 mV at 10, 100, 300 and 500 mA cm^{-2} in 1.0 M KOH, respectively, as well as excellent stability during 240 h at 100 mA cm^{-2}.

Experimental

Materials preparation

Ni foam (NF) was used as the substrate. The Ni foam was sonicated in ethanol, acetone and hydrochloric acid for 10 min, respectively, to remove grease and generate a rough surface. Then it was washed with deionized water and subsequently dried under vacuum at 60 °C. The in-situ electrochemical activation process was first conducted at a current density of 2 A cm^{-2} for 3 h in three concentrations of electrolytes (1.0 M, 6.0 M, and 10.0 M KOH) to optimize the concentration of electrolytes (Fig. S1). Then, the electrodes were activated at a serial of current density 1 A cm^{-2}, 2 A cm^{-2} and 3 A cm^{-2} for 3 h, respectively, in the selected alkaline solution using a two-electrode setup. The Ni foam (0.5 cm × 1 cm) was used as the anode and a graphite plate (1 cm × 5 cm) was used as the cathode. The obtained Ni foam electrodes activated at a current density of 1 A cm^{-2}, 2 A cm^{-2} and 3 A cm^{-2} were denoted as NF-1, NF-2, and NF-3, respectively.

Physicochemical characterizations

X-ray diffraction (XRD) patterns were recorded on a Bruker AXS D8 diffractometer using Cu Kα1 radiation ($\lambda = 0.15405$ nm) and Ni filter with 2θ ranging from 5° to 80° with a step size of 0.02° (1.0 s per step) at 40 kV. X-ray photoelectron spectroscopy (XPS) was performed with a PHI quantum-2000 (monochromatic Al Kα with 1486.6 eV operating at 15 kV and 300 W). The morphologies and energy dispersive spectroscopy (EDS) were performed on an FEI/Philips XL30 FEG scanning electron microscopy (SEM). Micro-Raman spectroscopy measurements were performed on a LabRAM™ system (Horiba Scientific, France) using a 532 nm (power <150 mW) laser diode as the excitation source.

Electrochemical characterization

All the electrochemical properties were characterized using an Autolab electrochemical workstation at room temperature (25 °C). A three-electrode system with a graphite plate (1 cm × 5 cm) as the counter electrode and a Hg/HgO electrode (Tianjin Aida Hengsheng Technology Co. Ltd., China) as the reference electrode was used. The activated Ni foam was used as the working electrode. To evaluate the electrocatalytic activity of the OER, cyclic voltammograms were recorded at 10 mV s^{-1} in the potential range between 0.98 and 1.73 V *vs.* RHE in oxygen-saturated 1.0 M KOH solution. The long-term stability was evaluated by chronoamperometry at 100 mA cm^{-2} in 1.0 M KOH solution. EIS measurements were recorded in a frequency range from 100 kHz to 0.1 Hz with an amplitude of 5 mV (peak-to-peak) at an applied potential of 1.56 V *vs.* RHE.

Results and discussion

The electrochemical activation process of the NF is illustrated in Scheme 1. In this process, the NF is electrochemically activated in-situ at different current densities (1 A cm^{-2}, 2 A cm^{-2} and 3 A cm^{-2} for 3 h, respectively) in a two-electrode system. The resulting electrodes are denoted as NF-1, NF-2, and NF-3, respectively. There are three reactions occurring at the anode (Scheme 1). At such high current densities, most of the current go-to the oxygen evolution reaction. Besides this, the surface Ni sites are oxidized to Ni^{2+} and react with OH^- to

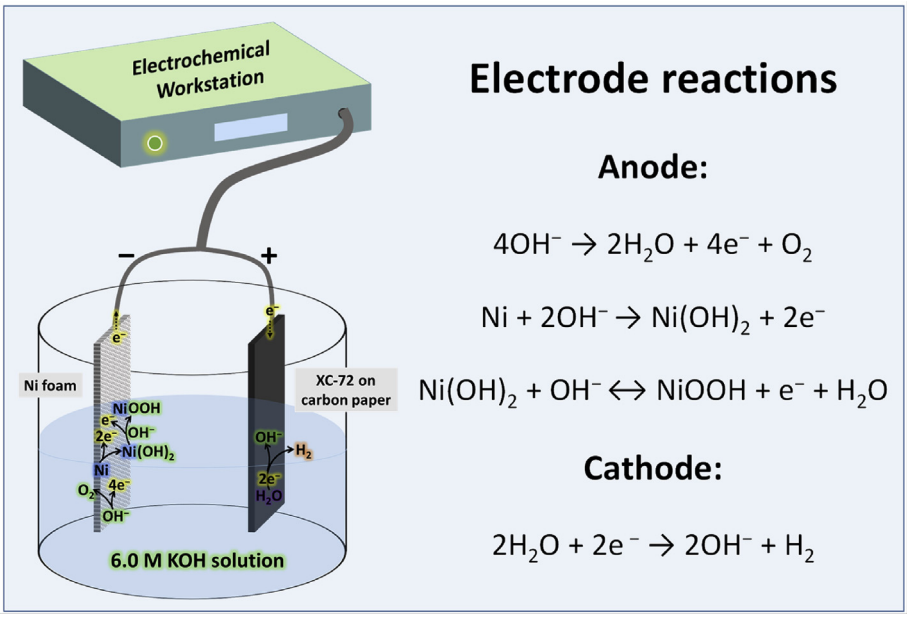

Scheme 1 – Schematic illustration and electrode reactions during the electrochemical activation of Ni foam.

form $Ni(OH)_2$ [40]. The $Ni(OH)_2$ then further oxidizes to Ni (oxy) hydroxide [40].

Scanning electron microscopy (SEM) shows that there are cracks on the surface of the NF electrodes, which is due to the acid pre-treatment (Fig. 1a–b, Figs. S2–S3). The NF-2 exhibits a rough surface, which is beneficial for electrocatalysis. Oxygen was uniformly distributed on the surface of the Ni foam, and the O content increased with increasing electrochemical activation current density from 1 to 3 A cm^{-2} (Fig. 1c). This indicates an increased thickness of the oxide film on the surfaces of the NF electrodes, which confirms the formation of Ni (oxy)hydroxide. The Raman peaks at 464 and 538 cm^{-1} are attributed to the combination peaks of $Ni(OH)_2$ and γ-NiOOH, while the broad peaks at around 900–1150 cm^{-1} were assigned to γ-NiOOH [41–43]. X-ray diffraction (XRD) was employed to detect the crystal structure of the electrocatalyst (Fig. S4). The 2θ diffraction peaks at 44.6°, 51.8°, and 76.5° correspond to the (111), (200), and (220) planes of cubic Ni

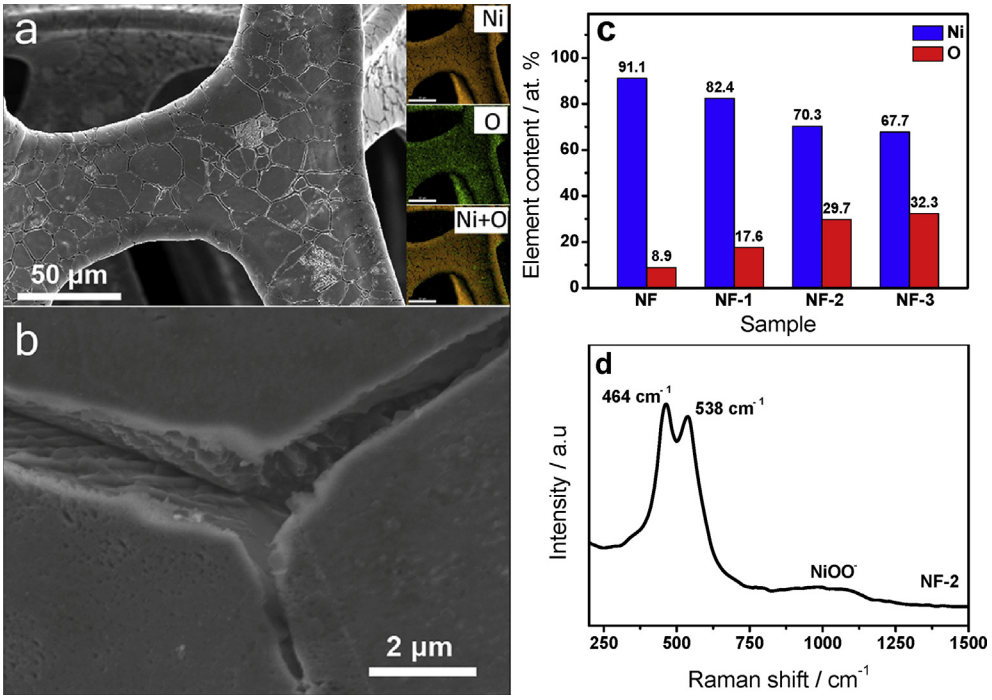

Fig. 1 – (a) SEM image and elemental mapping results of NF-2; (b) SEM image of the NF-2 at higher resolution (scale bar: 2 μm) (c) Elemental content of the activated NF electrode surfaces based on the EDS result; (d) Raman spectrum of the activated Ni foam electrode.

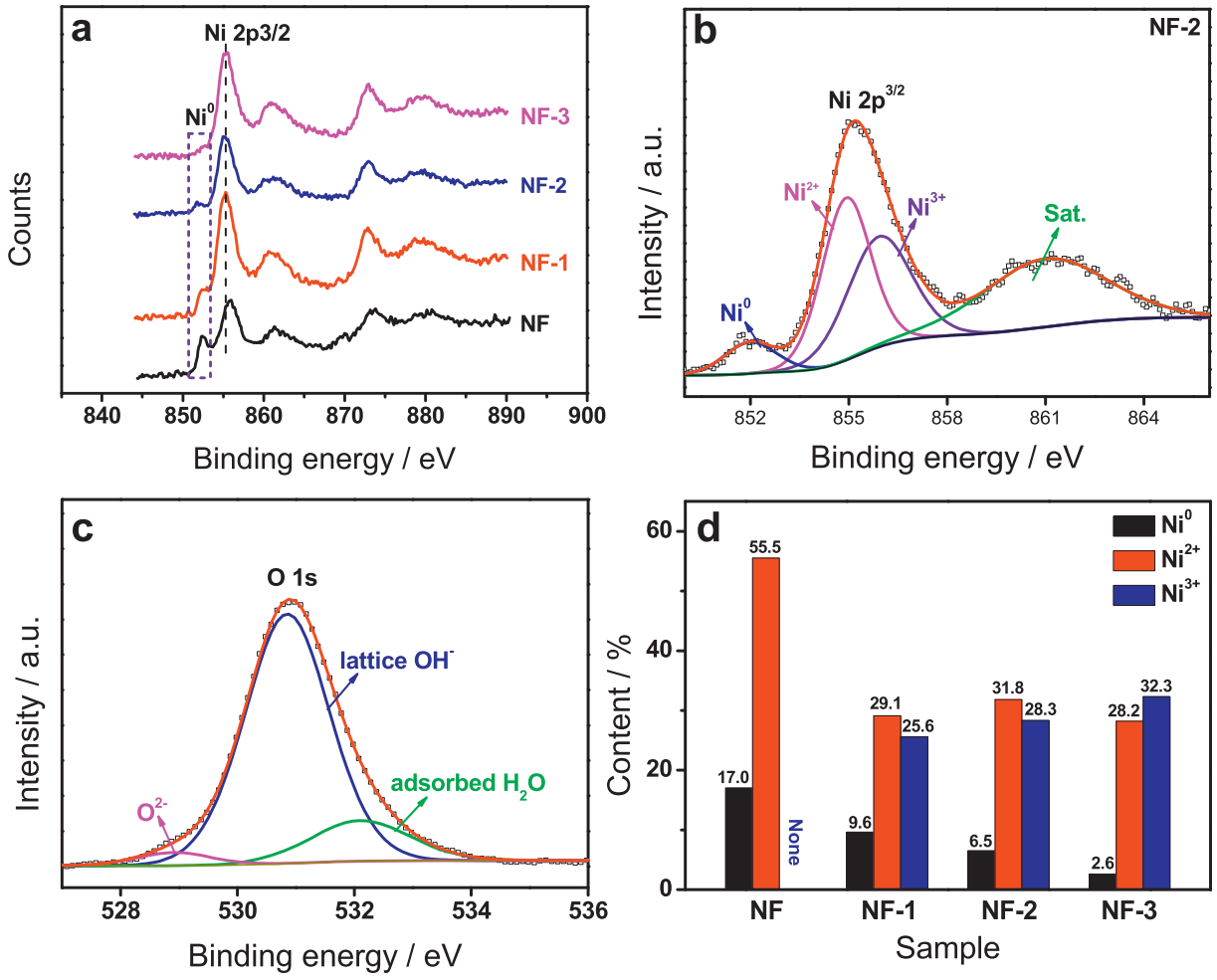

Fig. 2 – (a) High-resolution XPS peaks of Ni $2p_{3/2}$ for all samples; (b) Ni $2p_{3/2}$ peak and the peak fitting results for NF-2; (c) O 1s peak and the peak fitting results of NF-2; (d) Elemental content of Ni^{2+} and Ni^{3+} of the NF electrodes.

(JCPDS: 01-077-8341), respectively [44]. However, no diffraction peaks of Ni (oxy)hydroxide were identified, which may be due to its amorphous state or low crystallinity. This result is consistent with previous reports [43,44].

To further investigate the surface elemental composition and chemical changes of the NF electrode during the electrochemical activation, X-ray photoelectron spectroscopy (XPS) measurements were performed. The survey spectra indicate the presence of Ni and O on the surface of the NF electrodes (Fig. S5). The O content increased with the increased activation current density from 1 to 3 A cm^{-2}, consistent with the EDS result (Fig. 1c). Fig. 2 shows the Ni 2p peaks of the NF electrodes. The Ni 2p peaks at 855.9 eV, 873.4 eV, and 861.5/880.1 eV were assigned to the Ni $2p_{3/2}$, Ni $2p_{1/2}$, and satellite peaks, respectively. All of the electrochemically activated NF electrodes show a negative shift (0.5 eV) of binding energy compared to the inactivated NF, indicating strong electronic interactions between the surface Ni (oxy)hydroxide and the NF substrate [45,46], which favors electron transfer during OER.

The peaks at 852.5 eV correspond to Ni $2p_{3/2}$ of the metallic Ni^0, which is attributed to the Ni foam substrate [47]. Obviously, the intensity of the metallic Ni^0 peaks decreased with increasing activation current density due to the growth of the (oxy)hydroxide film on the surface of the NF electrodes. The Ni $2p_{2/3}$ and O 1s spectra of the activated NF electrodes were further deconvoluted (Fig. 2b and c, Fig. S6). For the Ni $2p_{2/3}$, the three peaks at 852.5 eV, 854.9 eV, and 855.9 eV correspond to different Ni valences of Ni^0, Ni^{2+}, and Ni^{3+}, respectively [47–50]. The O 1s peaks were deconvoluted into three peaks located at 528.9 eV for the lattice oxygen O^{2-}, 530.9 eV for lattice OH^- bond, and 532.4 eV for adsorbed H_2O molecules [33,51–53]. These results further confirm the formation of Ni (oxy)hydroxide during the electrochemical activation process. Fig. 2d summarizes the content of Ni^0, Ni^{2+}, and Ni^{3+}on the surface of the NF electrodes. It is seen that the content of Ni^{3+} slightly increased with increasing activation of current density from 1 to 3 A cm^{-2}. Based on the above-mentioned results, the activated NF electrodes are expected to show an enhanced OER activity.

The electrocatalytic activity of the NF electrodes toward OER was investigated in 1.0 M KOH (Fig. 3a). The peaks at 1.37 V and 1.29 V *vs.* RHE was assigned to the redox reaction of $Ni^{2+} \rightleftharpoons Ni^{3+}$ that goes forward and backward, respectively [54,55]. When scanning to more positive potentials, the current density rapidly increases due to oxygen evolution [35]. It

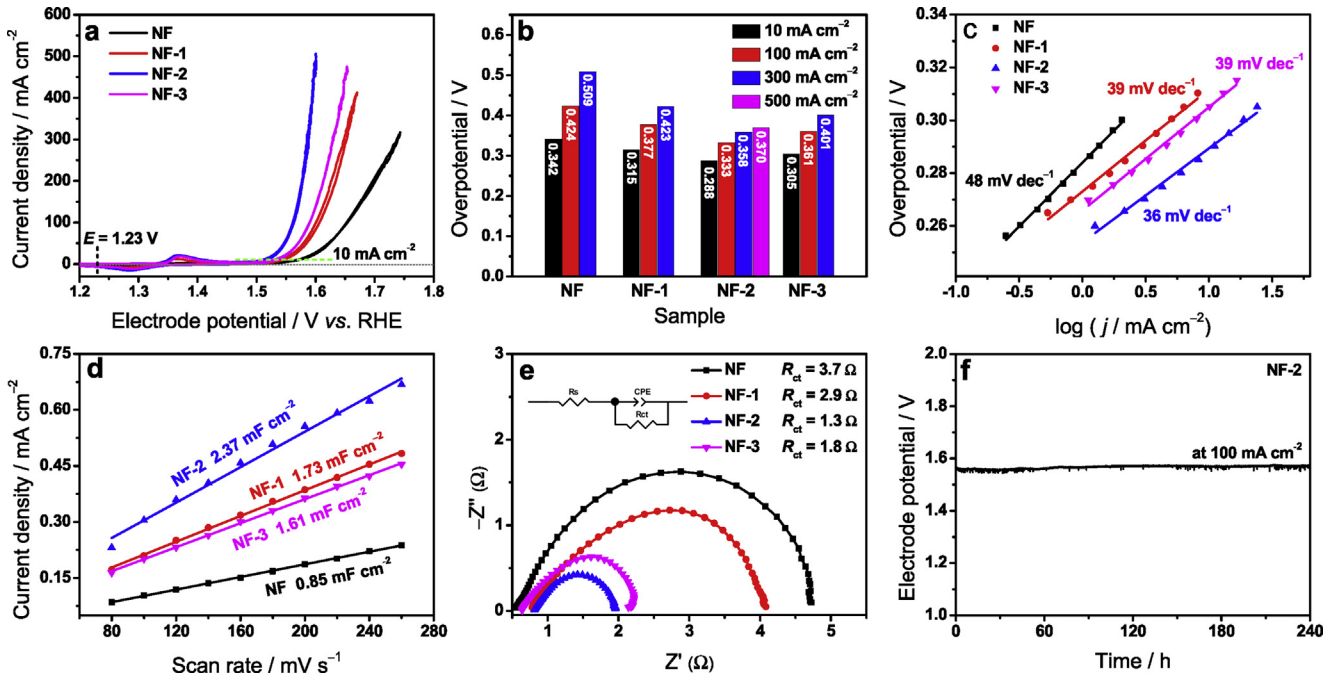

Fig. 3 – (a) Cyclic voltammograms of the NF electrodes in 1.0 M KOH at a scan rate of 10 mV s^{-1}; (b) The corresponding overpotentials at different current densities extracted from Fig. 3b; (c) The corresponding Tafel plots of NF electrodes in 1.0 M KOH; (d) Plot of current densities versus scan rates for the NF electrodes at the electrode potential of 0.82 V vs. RHE, from which the electrical double layer capacitance (C_{dl}) of the NF electrodes were derived from the slope; (e) Nyquist plots and fitting results of the catalysts in the frequency range from 100 kHz to 0.1 Hz with an amplitude of 5 mV at 1.56 V *vs.* RHE (Inset is the equivalent circuit, where R_s is the resistance of the electrolyte, R_{ct} is the charge transfer resistance, and CPE is a constant phase element); (f) Stability test of the NF-2 electrode at 100 mA cm^{-2} in 1.0 M KOH.

is found that all electrochemically activated NF electrodes exhibit a significant improvement in OER activity. The overpotential (η) at a current density of 10 mA cm^{-2} was employed to evaluate the electrocatalytic activity of OER [56]. The overpotential at 10 mA cm^{-2} of the NF electrodes follows the order: NF-2 < NF-3 < NF-1 < NF (Fig. 3b). The NF-2 electrode displayed an overpotential of 288 mV at 10 mA cm^{-2}, which is one of the best performing OER catalysts reported in the literature (Table S1). In particular, the NF-2 achieved a current density as high as 500 mA cm^{-2} at an overpotential of 370 mV, making it a promising anode electrocatalyst for practical applications of water splitting. The Tafel slopes of the activated NF electrodes were around 40 mV dec^{-1} (Fig. 3c), indicating that the OER process may be controlled by the formation of *-O of the Krasil'shcikov path [57–59]. The Faradaic efficiency of the NF-2 electrode for the OER was found to be around 99%, indicating that nearly all of the current was used for the evolution of oxygen (Fig. S7).

In order to further insight into the activity of the electrodes, the electrical double layer capacitance (C_{dl}) of the NF electrodes was extracted from the slope of the plot of current densities versus scan rates at the electrode potential of 0.82 V *vs.* RHE (Fig. 3d, Fig. S8). The C_{dl} is usually employed to evaluate the electrochemically active area of the electrodes during electrocatalysis. A higher C_{dl} means better access of electrolyte to the active sites. It is seen that all of the activated NF electrodes exhibit a larger C_{dl} than the original NF, which is attributed to the formation of Ni (oxy)hydroxide species (Figs. 1d and 2) thus increasing the active area of the NF electrodes, consistent with the OER activity (Fig. 3a). The NF-2 electrode exhibits the highest C_{dl} of 2.37 mF cm^{-2}, which is nearly three times that of the untreated NF electrode (0.85 mF cm^{-2}). While the NF-3 electrode with a high content of Ni (oxy)hydroxide species shows a lower C_{dl} value than that of NF-1 and NF-2. This may be attributed to the destruction of the NF surface structure at such a high current density of 3 A cm^{-2} thus decreasing the electrochemically active area. Moreover, the charge transfer resistance (R_{ct}) of the NF electrodes for the OER was evaluated by electrochemical impedance spectroscopy (EIS) at an applied potential of 1.56 V *vs.* RHE (Fig. 3e). It is found that all of the electrodes exhibit low R_{ct} (1.3 Ω for NF-2, 1.8 Ω for NF-3, 2.9 Ω for NF-1), which is attributed to the direct formation of Ni (oxy)hydroxide on the NF electrodes without using any (non-conductive) binder. The NF-2 electrode displays the lowest charge transfer resistance of 1.3 Ω. Due to the large content of nickel (oxy)hydroxide species, highest active area and lowest charge transfer resistance, the NF-2 electrode exhibits the best OER activity among the tested NF electrodes.

Finally, the NF-2 was selected to perform at 100 mA cm^{-2} for 240 h, which exhibits excellent long-term stability with negligible potential increase over 240 h at100 mA cm^{-2} (Fig. 3f). After the OER test, there were no changes in the structure of the sample (Fig. S9). The oxygen content was further increased after long-term stability tests, which may be attributed to the oxidation of the nickel foam during the OER test (Fig. S10).

Conclusions

In summary, an electrochemical activation method was developed for the in-situ formation of Ni (oxy)hydroxide on the surface of Ni foam electrodes in alkaline media. The obtained NF-2 electrode exhibits highly electrocatalytic activity for the OER with an overpotential of 288 mV at 10 mA cm^{-2} and 370 mV at 500 mA cm^{-2}, respectively, as well as excellent long-term stability at 100 mA cm^{-2} over 240 h. The outstanding OER performance is attributed to the highly active Ni (oxy)hydroxide, large electrochemically active area, and low charge transfer resistance and interfacial electronic resistance. This work provides an easy and marketable strategy for the preparation of highly active and stable OER electrocatalysts for a future hydrogen economy.

Acknowledgements

K. Wan is grateful to the Oversea Study Program of Guangzhou Elite Project. X. Zhang is grateful to Research Fund KU Leuven for a postdoctoral fellowship (PDM-short term). J. Luo acknowledges the Research Foundation – Flanders (FWO) for a Research Project (G0B3218N) and the Discipline Development Research Project of Think Tank for Fujian Provincial Association for Science and Technology (project number: FJKX-XK1722). Funding from the National Natural Science Foundation of China (No. 21776120) and Natural Science Foundation of Fujian Province, China (project No.: 2018J01433) is acknowledged. The Open Project Program of Provincial Key Laboratory of Clean Energy Materials, Longyan University (QJNY-201705) is also acknowledged.

Appendix A. Supplementary data

Supplementary data to this article can be found online at https://doi.org/10.1016/j.ijhydene.2020.01.043.

REFERENCES

[1] You B, Sun Y. Accounts Chem Res 2018;51:1571–80.
[2] Xiang ZP, Deng HQ, Peljo P, Fu ZY, Wang SL, Mandler D, Sun GQ, Liang ZX. Angew Chem Int Ed 2018;57:3464–8.
[3] Zhu W, Zhang R, Qu F, Asiri AM, Sun X. ChemCatChem 2017;9:1721–43.
[4] Liang Z, Ahn HS, Bard AJ. J Am Chem Soc 2017;139:4854–8.
[5] Li P, Zhao R, Chen H, Wang H, Wei P, Huang H, Liu Q, Li T, Shi X, Zhang Y. Small 2019;15:1805103.
[6] Long GF, Wan K, Liu MY, Liang ZX, Piao JH, Tsiakaras P. J Catal 2017;348:151–9.
[7] Chen HY, Jin MX, Zhang L, Wang AJ, Yuan J, Zhang QL, Feng JJ. J Colloid Interface Sci 2019;543:1–8.
[8] Chen Y, Zheng XX, Huang XY, Wang AJ, Zhang QL, Huang H, Feng JJ. J Colloid Interface Sci 2020;559:206–14.
[9] Niu H-J, Chen H-Y, Wen GL, Feng JJ, Zhang QL, Wang AJ. J Colloid Interface Sci 2019;539:525–32.
[10] Liu B, Wang C, Chen Y, Ma B, Zhang J. Int J Hydrogen Energy 2019;44:511–22.
[11] Shi Y, Lu Z, Guo L, Wang Z, Guo C, Tan H, Yan C. Int J Hydrogen Energy 2018;43:9133–43.
[12] Lim J, Yang S, Kim C, Roh CW, Kwon Y, Kim YT, Lee H. Chem Commun 2016;52:5641–4.
[13] Du X, Zhang X, Li Y, Zhao M. Int J Hydrogen Energy 2018;43:19955–64.
[14] Zhang X, Luo JS, Lin HF, Tang PY, Morante JR, Arbiol J, Wan K, Mao BW, Liu LM, Fransaer J. Energy Storage Mater 2019;17:46–61.
[15] Gorlin M, Chernev P, Paciok P, Tai CW, Ferreira de Araujo J, Reier T, Heggen M, Dunin-Borkowski R, Strasser P, Dau H. Chem Commun 2019;55:818–21.
[16] Li C, Chen J, Wu Y, Cao W, Sang S, Wu Q, et al. Int J Hydrogen Energy 2018;44:2656–63.
[17] Zhong HX, Wang J, Zhang Q, Meng F, Bao D, Liu T, Yang XY, Chang ZW, Yan JM, Zhang XB. Adv Sustain Syst 2017;1:1700020.
[18] Du X, Wang Q, Li Y, Zhang X. Dalton Trans 2018;47:10273–80.
[19] Burke MS, Enman LJ, Batchellor AS, Zou S, Boettcher SW. Chem Mater 2015;27:7549–58.
[20] Zhang X, Luo J, Wan K, Plessers D, Sels B, Song J, Chen L, Zhang T, Tang P, Morante JR, Arbiol J, Fransaer J. J Mater Chem 2019;7:1616–28.
[21] Wan K, Luo J, Zhang X, Zhou C, Seo JW, Subramanian P, Yan JW, Fransaer J. J Mater Chem 2019;7:19889–97.
[22] Du X, Su H, Zhang X. ACS Sustainable Chem Eng 2019;7:16917–26.
[23] Du X, Yang Z, Li Y, Gong Y, Zhao M. J Mater Chem 2018;6:6938–46.
[24] Zheng Y, Zhang L, Huang H, Wang F, Yin L, Jiang H, Wang D, Yang J, Zuo G. Int J Hydrogen Energy 2019;44:27465–71.
[25] Jia X, Wang M, Liu G, Wang Y, Yang J, Li J. Int J Hydrogen Energy 2019;44:24572–9.
[26] Liu Q, Xie L, Liu Z, Du G, Asiri AM, Sun X. Chem Commun 2017;53:12446–9.
[27] Xiong X, You C, Liu Z, Asiri AM, Sun X. ACS Sustainable Chem Eng 2018;6:2883–7.
[28] Wu D, Wei Y, Ren X, Ji X, Liu Y, Guo X, Liu Z, Asiri AM, Wei Q, Sun X. Adv Mater 2018;30:1705366.
[29] Zhao J, Li X, Cui G, Sun X. Chem Commun 2018;54:5462–5.
[30] Niu HJ, Wang AJ, Zhang L, Guo JJ, Feng JJ. Mater Chem Front 2019;3:1849–58.
[31] Jin MX, Pu YL, Wang ZJ, Zhang Z, Zhang L, Wang AJ, et al. ACS Appl Energy Mater 2019;2:4188–94.
[32] Görlin M, Chernev P, Ferreira de Araújo J, Reier T, Dresp S, Paul B, Krähnert R, Dau H, Strasser P. J Am Chem Soc 2016;138:5603–14.
[33] Wang HY, Hsu YY, Chen R, Chan TS, Chen HM, Liu B. Adv Energy Mater 2015;5:1500091.
[34] Tahir M, Pan L, Zhang R, Wang YC, Shen G, Aslam I, Qadeer MA, Mahmood N, Xu W, Wang L, Zhang X, Zou JJ. ACS Energy Lett 2017;2:2177–82.
[35] Wan K, Luo J, Zhou C, Zhang T, Arbiol J, Lu X, Mao BW, Zhang X, Fransaer J. Adv Funct Mater 2019;29:1900315.
[36] Li B, Ge X, Goh FT, Hor TA, Geng D, Du G, Liu Z, Zhang J, Liu X, Zong Y. Nanoscale 2015;7:1830–8.
[37] Zhang X, Luo JS, Tang PY, Ye XL, Peng XX, Tang HL, Sun SG, Fransaer J. Nano Energy 2017;31:311–21.
[38] Gu W, Hu L, Zhu X, Shang C, Li J, Wang E. Chem Commun 2018;54:12698–701.
[39] Guo CX, Li CM. Chem Commun 2018;54:3262–5.
[40] Chung YH, Jang I, Jang JH, Park HS, Ham HC, Jang JH, Lee YK, Yoo SJ. Sci Rep 2017;7:8236.
[41] Trześniewski BJ, Diaz-Morales O, Vermaas DA, Longo A, Bras W, Koper MTM, Smith WA. J Am Chem Soc 2015;137:15112–21.
[42] Diaz-Morales O, Ferrus-Suspedra D, Koper MTM. Chem Sci 2016;7:2639–45.

[43] Jin Y, Huang S, Yue X, Du H, Shen PK. ACS Catal 2018;8:2359–63.
[44] Wang J, Zhang W, Zheng Z, Liu J, Yu C, Chen Y, Ma K. Appl Surf Sci 2019;469:731–8.
[45] Zheng M, Du J, Hou B, Xu CL. ACS Appl Mater Interfaces 2017;9:26066–76.
[46] Yu J, Cheng G, Luo W. J Mater Chem 2017;5:15838–44.
[47] Hao S, Chen N, Liu Q, Xie Y, Fu H, Yang Y. Chem Asian J 2018;13:944–9.
[48] Lian K, Thorpe S, Kirk D. Electrochim Acta 1992;37:2029–41.
[49] Lian K, Kirk D, Thorpe S. J Electrochem Soc 1995;142:3704–12.
[50] Li CP, Proctor A, Hercules DM. Appl Spectrosc 1984;38:880–6.
[51] Yan Z, Sun H, Chen X, Liu H, Zhao Y, Li H, Xie W, Cheng F, Chen J. Nat Commun 2018;9:2373.
[52] Li F, Du J, Li X, Shen J, Wang Y, Zhu Y, Sun L. Adv Energy Mater 2018;8:1702598.
[53] Luo W, Jiang C, Li Y, Shevlin SA, Han X, Qiu K, Cheng Y, Guo Z, Huang W, Tang J. J Mater Chem 2017;5:2021–8.
[54] Thangasamy P, Maruthapandian V, Saraswathy V, Sathish M. Catal Sci Technol 2017;7:3591–7.
[55] Wu LK, Wu WY, Xia J, Cao HZ, Hou GY, Tang YP, Zheng GQ. J Mater Chem 2017;5:10669–77.
[56] Luo JS, Im JH, Mayer MT, Schreier M, Nazeeruddin MK, Park NG, Tilley SD, Fan HJ, Gratzel M. Science 2014;345:1593–6.
[57] Miller EL, Rocheleau RE. J Electrochem Soc 1997;144:3072–7.
[58] Xiao H, Shin H, Goddard WA. Proc Natl Acad Sci USA 2018;115:5872–7.
[59] Gupta S, Qiao L, Zhao S, Xu H, Lin Y, Devaguptapu SV, Wang X, Swihart MT, Wu G. Adv Energy Mater 2016;6:1601198.